Automatic Registration of Postmortem Brain Slices to MRI Reference Volume

T.-S. Kim†, M. Singh† *Senior Member, IEEE,* W. Sungkarat†,
C. Zarow*, and H. Chui*
†Depts. of Radiology and Biomedical Engineering, *Dept. of Neurology, University of Southern California

ABSTRACT

A new strategy to register each slice of the postmortem brain to anatomically corresponding in-vivo MRI slices is presented. The approach relies on a recursive reslicing of the MRI volume using non-linear polynomial transformations. Simulation studies to validate the approach and results using real data are presented. The results suggest the feasibility and practicability of second- and third-order polynomials to register postmortem images on a slice-by-slice basis to corresponding MRI sections. Using this method, it is possible to investigate the pathology of a disease through routinely acquired MRIs and postmortem brain images.

I. INTRODUCTION

The pathology of disease is generally studied by analyzing postmortem brain slices. However postmortem slices alone do not fully reflect the pathology of disease. Since Magnetic Resonance Imaging (MRI) is increasingly and commonly utilized in clinical evaluations, premortem MRI can be utilized to improve the identification and understanding of specific diseases by providing an objective quantification of pathology through MR signal characterization. For instance, patients with small-vessel ischemia and Alzheimer's disease show white matter lesions (WML), hippocampal and cortical atrophy, and peculiar vascular infarctions known as lacunar infarcts or lacunes [1]. Some of these characteristics cannot be identified on postmortem slices, but MRI detects significant abnormalities in cortical and subcortical regions. Thus correlating postmortem to in-vivo MR images would provide a better understanding of disease progression. Registering slices of the postmortem brain to the premortem MR images, however, is a challenging task for a number of reasons.

First, the interval between premortem MRI and postmortem brain generates structural discrepancy. There have been previous attempts to circumvent this issue by performing a postmortem MRI [2]. However it is known that MRI signal characteristics alter dramatically in the postmortem brain. For example, the T2-weighted signals are found to decay within the first 90 hours after death [3]. Thus relating postmortem MRIs to premortem MRIs is itself a difficult problem.

Second, the slices of postmortem brain are prone to geometrical distortions due to slicing, dehydration, and structural deformation. This is because the brain is subject to multiple deformations at the time of death. The brain swells during the agonal state and shrinks during fixation. After removal from the cranial vault, the ventricles collapse and the brain becomes severely deformed.

Third, variability also occurs in the planar thickness and orientation of postmortem slices, making it difficult to keep all the slices with respect to a single reference point to realign the images. This makes 3D-volume reconstruction difficult.

Previous attempts to correlate MRI and the postmortem brain have been limited to local structures of interest imaged and sectioned in corresponding planes [4-6]. To our knowledge, no slice-by-slice comparisons have been made. Even though the postmortem-to-MRI registration process presents several difficulties, it is clear that such correlations would provide a very powerful means to investigate the pathology of disease.

In most currently available image registration techniques, coregistration is performed in 3D, matching one image volume to the other, and then slices are derived from the registered volumes. To compensate for geometrical mismatch in 3D, image warping is incorporated to redefine the spatial relationships among voxels in a volume. Image-warping approaches can be classified in general as intensity-based and model-based strategies to produce 3D linear and non-linear deformations [7]. For instance, intensity-based registration routines such as Automatic Image Registration (AIR) [8] perform well with high-resolution 3D image volumes and relatively comparable voxel characteristics such as PET-to-PET, MRI-to-MRI, or PET-to-MRI. Model-based approaches generally require points, curves, and surface-based representation of structures.

The current image registration approaches perform efficiently if evenly sliced and orientation-preserved slices are available such that an accurate 3D reconstruction of the image volume is possible. Application of existing registration methods to postmortem-MRI coregistration is limited by the difficulty in forming accurate 3D-volumes and severe geometrical distortions. Furthermore, generating structural models require human interactions since such models are not readily available for pathological state-changing postmortem images. Thus, a new approach is needed for postmortem-MRI coregistration.

In this study we present a new strategy to register each slice of the postmortem brain to its corresponding MRI on a slice-by-slice basis using 2D-to-3D mapping afforded by non-linear polynomial transformations. Each slice of the warped MR image is derived recursively from a reference MR volume using non-linear polynomials. Validation studies with simulated data and results of registering real data are presented in this paper.

II. METHOD

A. Postmortem Brain Image Preparation

The postmortem brains were fixed in 10% neutral formalin for at least two weeks, and then each brain was sectioned into 25-30 5mm thick coronal slices using a motor-driven rotary slicer. Each image was then digitized and stored in the Kodak PhotoCD RGB color format at a resolution of 3072x2048 (Fig.

0018-9499/00$10.00

1), keeping an in-plane spatial resolution of approximately 0.6mm.

B. Premortem Magnetic Resonance Imaging

To facilitate visualization of lacunes (which are best seen in relatively thick transaxial proton density and T2 weighted slices) and other structures such as the hippocampus (which are best seen in relatively thin T1 weighted coronal slices) three types of data sets were acquired on a GE 1.5T Signa System: coronal T1-weighted, transaxial Proton Density (PD), and transaxial T2-weighted MRIs respectively.

The T1-weighted 3D coronal scan was made using a gradient-echo (SPGR) sequence with TR=24ms, TE=5ms, flip angle=45°, field of view=24x24cm^2, 124 slices, slice thickness=1.5mm, and 0.86x0.86 mm^2 in-plane resolution. The PD and T2-weighted images were acquired using a dual-echo turbo spin echo (TSE) sequence with TR=45ms, TE1=14ms, TE2=85ms, 51 slices, slice thickness=3mm, and 1.0x1.0mm^2 in plane resolution.

C. Brain Segmentation

The brain was extracted from the background of RGB postmortem images by selectively thresholding RGB intensity values, then stored in gray scale. The Brain Surface Extraction (BSE) Algorithm developed by Sander and Leahy [9], which extracts brain regions using a morphological algorithm, was used to strip off the skull and scalp of the MR images. In addition, the regions of pons and cerebrum were removed manually by inspecting each MR slice, since these regions were absent in the postmortem slices.

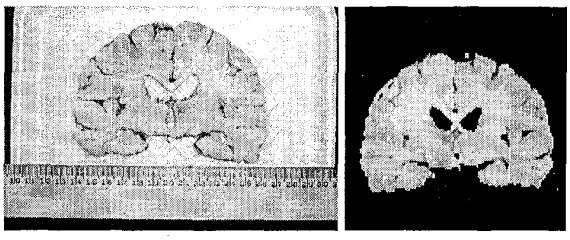

Figure 1: Photograph of a postmortem slice (left) and its gray-scale version after removal of the background (right). The gray-scale image was flipped left-to-right to match MRI orientation.

D. Image Registration

The purpose of this work is to relate MR signal characteristics (T1, T2, and PD) derived from transaxial or coronal images to corresponding lesions or regions of interest (ROI) in the postmortem images by matching postmortem slices to MRI sections lying within the MRI volume. Since only a few slices of postmortem images contain regions of interest or lesions, the approach of matching slices instead of the entire postmortem volume is cost effective. Also better sensitivity in matching images can be obtained because only one postmortem slice is considered at a time. Due to its higher resolution, a set of coronal T1-weighted MR images was used to form a referential volume.

The severe geometrical distortions in the postmortem images makes it necessary to use image warping for co-registration. Warping was incorporated by a coordinate transformation from 2D to 3D coordinates using modified general nth-order polynomials in the following manner [10]:

$$\begin{aligned} u &= a_0 + a_1 x + a_2 y + a_3 x^2 + a_4 xy + a_5 y^2 + \ldots \\ v &= b_0 + b_1 x + b_2 y + b_3 x^2 + b_4 xy + b_5 y^2 + \ldots \\ w &= c_0 + c_1 x + c_2 y + c_3 x^2 + c_4 xy + c_5 y^2 + \ldots \end{aligned} \quad (1)$$

In the above equations, x and y are indices of the 2D image, u, v and w are coordinates of a pixel in the 3D reference volume image, and a_i, b_i and c_i are the coefficients of image transformation.

This polynomial transformation translates the coordinates of pixels in the 2D postmortem slice to voxels in the 3D MRI volume. The registration algorithm was designed to take an initial MR slice that produced the minimum error, and then transformation parameters were estimated using a quasi-Newton-based multidimensional optimization algorithm [11]. A linear or cubic 3D interpolation method [11] was used to produce an image at the transformed voxel coordinates. Beginning with the initial location within the MRI volume as shown in Fig. 2, a warped 2D section lying within the 3D MRI volume was derived at every iteration until a MR section matching a postmortem slice was found. The best match between a MR section and a postmortem image was found by minimizing the error between the recursively sliced and warped MR section and a given postmortem slice.

Two different cost criteria were investigated to determine the registration error between a postmortem slice and a registered MRI section. Based on our registration work in functional MRI [12] and its proven effectiveness in AIR [8], first we derived a cost function from the variance over mean of voxel intensity ratios between the two images. However, this approach did not work well in our initial studies, mainly due to the extreme distortions and nonuniform pixel intensity distribution between the postmortem and MR images. In the work reported here, we utilized the mean-squared error (MSE) as a minimizing cost, leading to the following objective function to minimize for estimating the optimal parameters a_i, b_i and c_i:

$$\min \; f(a_i, b_i, c_i) = \sum_{j=1}^{N} \left\| X_j - Y_j \right\|^2 \quad (2)$$

where i is the index of polynomial coefficients, and X_j and Y_j are voxel intensities with index j.

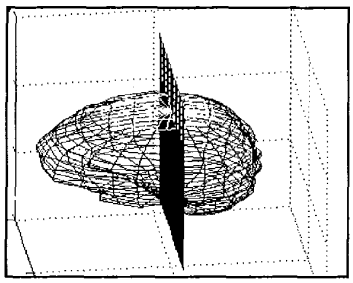

Figure 2: Location of the initial MR slice within the 3D MR volume. A warped section around this slice is derived from the use of modified nth-order polynomials.

E. Registration in Different Orientation

In certain cases, it is easier to localize a targeted region in a slice orientated differently from the slices used to form the 3D volume. Then the registration problem becomes a two-step procedure, registration of MRI-to-MRI in the first step and registration of MRI-to-postmortem images in the second step.

Registration of a MRI slice oriented differently (e.g., transaxial) from slices used to form the 3D volume (e.g., coronal) can be performed by a polynomial transformation in a manner similar to that described for the single postmortem slice to 3D volume registration. Once the transformation is completed, the coordinates of the targeted region, e.g., a lesion in the transaxial plane, can be transformed into coordinates of voxels in the 3D reference volume using the coefficients of the transformation. Thus if (x_j, y_j) are pixel coordinates of lesions before registration, the coordinates of lesion voxels after registration (u_j, v_j, w_j) within the 3D MRI can be found from the following equation:

$$(u_j, v_j, w_j) = P(a_i, b_i, c_i, x_j, y_j) \qquad (3)$$

where P represents the n^{th}-order polynomial.

Marked lesions in 3D MRI can then be related to coordinates in the post-mortem slices by registering several postmortem slices one-by-one to the MRI volume till the marked coordinates in the MRI volume lie within a warped MRI section corresponding to a particular postmortem slice.

F. Computer Simulation

To validate the registration procedure numerically, computer simulation studies were conducted using an experimentally acquired 3D MRI volume as a reference. First, a coronal MRI slice was selected from near the middle of the reference volume. Next a 4^{th}-order polynomial was used to form a warped section around this slice to simulate the distortions that might occur when the brain is taken out of the skull and sliced. The coefficients of the 4^{th}-order polynomial were selected to produce a deformed image that had the visual appearance of a typical post-mortem slice. This simulated post-mortem slice was then registered to the 3D MR volume using second- and third-order polynomials as described before. The ventricle regions were masked manually and excluded from the registration cost function analysis to simulate the effect of severe distortions within these regions.

G. Validation via Anatomical Landmarks

In addition to numerical validation, the reliability and accuracy of the registration method was also tested through identification of common anatomical landmarks (e.g., anterior commissure, pillars of fornix, perivascular spaces, and optic chiasm) between the postmortem and MR images.

III. Results

A. Computer Simulation Studies

Fig. 3 (a) shows a typical MRI coronal slice selected from near the middle of the 3D volume. This coronal image contains no distortion and represents a reference slice within the volume. A 4^{th}-order deformed image derived from the MRI volume is shown in Fig. 3 (b). After masking a region around the ventricles (shown by the dotted lines) from the registration cost, the MR sections that matched Fig. 3 (b) using 2^{nd}- and 3^{rd}-order polynomials are shown in Figs. 3 (c) and (d) respectively. To assess the accuracy of registration, we utilized two voxel intensity based measures, the correlation coefficient (cc) [10,13] and MSE. These two measures were also used in a recent study [13] to evaluate voxel similarity in registered images. The registered image in Fig. 3 (c) had a cc of 0.9952 with respect to the reference image, i.e., it accounts for 99.52 percents of the overall voxel intensity variations within the reference image. Fig. 3 (d) showed a higher cc of 0.9970 with respect to the reference image. Fig. 4 shows the convergence of the MSE using 2^{nd} and 3^{rd}-order polynomials. At convergence, the 3^{rd}-order registration produced lower MSE than the 2^{nd}-order registration, suggesting better registration with the 3^{rd}-order transformation in this example.

Three different mask sizes were tested to assess the sensitivity of masking. As the mask size (measured by the number of voxels lying inside the masked region) increased, cc decreased and MSE increased systematically in the following way MSE/cc/voxels: 7.0E5/0.9898/190, 1.4E6/0.9796/357, and 3.3E6/0.9526/657. Voxels contained within the masked region were included in the above computation of cc and MSE values. This implies a loss of registration sensitivity due to masking. However, when the voxels inside the mask were excluded from the computation, MSE decreased with the bigger masks, while cc remained almost constant: 1.1E5/0.9983/190, 1.0E5/0.9984/357, and 8.7E4/0.9987/650. These results suggest that the registration method is not very sensitive to the actual size of the mask used to exclude severely distorted pixels within the ventricular regions.

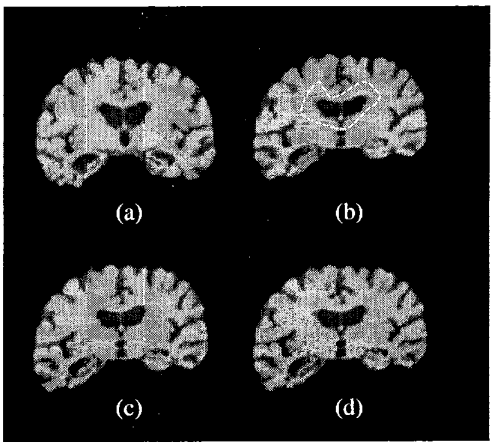

Figure 3: Simulation results. (a) Sliced MR image from 3D volume without any distortion. (b) MR image containing 4^{th}-order distortion, (c) MR image registered to 3(b) using 2^{nd}-order polynomials, and (d) MR image registered to 3(b) using 3^{rd}-order polynomials. The masked region in (b) was excluded from the registration cost.

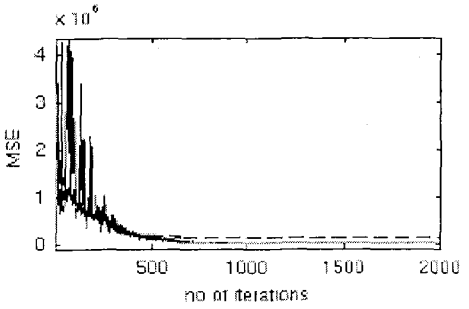

Figure 4: Convergence plot of 2nd-order (--) and 3rd-order (-) registrations corresponding to Figs. 3 (c) and (d) respectively.

B. Experimental Studies: 2nd-order Registration

Our preliminary studies to register postmortem images to the corresponding MR images using rigid-body transformation (i.e., linear affine transformation) suggested that distortions in postmortem slices could not be compensated with linear transformations. A 2nd-order polynomial non-rigid transformation was used to obtain the results shown below.

Fig. 5 (a) shows a typical postmortem image. Severe structural deformation is visible in the ventricles. The registration algorithm was initialized with a coronal MR slice shown in Fig. 5 (b) that produced the minimum MSE with respect to the postmortem image. Starting with this image, Fig. 5 (c) was obtained from a warped reslicing of the MR volume at a convergence threshold typically set to be 1.0E-6. The correlation coefficient between Figs. 5 (c) and 5 (a) was 0.928 whereas cc between Figs. 5 (a) and (b) was 0.729. Fig. 5 (d) shows the difference image corresponding to 5(c)-5(a). As indicated by the gray-scale bar, positive differences are shown as brighter and negative differences as darker than the gray background.

The results of registering two consecutive postmortem slices to the volume MRI of another subject are shown in Fig. 6. The consecutive postmortem slices are shown in Fig. 6 (a) and (c), and the resulting MRI sections are shown in Figs. 6 (b) and (d), with correlation coefficients of 0.891 and 0.888 respectively. The registered MRIs clearly show different and non-overlapping slices of the MRI volume with distinctive structures of gyri and ventricles. This suggests that adjacent slices can be resolved with the technique.

To verify that the registered MRIs do contain the same anatomical structures originally found in the postmortem slices, we inspected the images for common anatomical features. As an example, we note that two anatomical landmarks, the perivascular spaces and optic chiasm, are both present in images shown in Figs. 6 (a) and (b). These matching structures are indicated by the same types of arrows in Fig. 6: the right arrows indicate perivasular space, and the left optic chiasm.

To test the sensitivity of our cost function with respect to the initial conditions, we initialized our algorithm with different slices. The first initial slice was selected if it produced minimum MSE with respect to the target slice, then other initial slices were selected 3-5 slices away (i.e., 4.5-6mm) from the first initial slice in both anterior and posterior directions. We confirmed that the algorithm converged to nearly identical parameters without significant changes in each situation. Note that we utilized the Newton-type based optimization method [11] that is more sensitive to initial conditions. Adopting other optimization methods such as the Simplex method [11] would make the algorithm more tolerant to initial conditions at the cost of computation time.

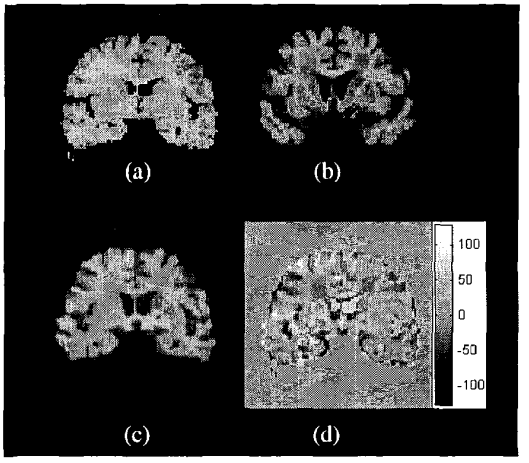

Figure 5: Results of coronal image registration using 2nd-order polynomial transformation. (a) A postmortem image (b) initial MRI for iterative registration (c) registered MRI, and (d) difference between postmortem and registered MR image, i.e., (c) minus (a). The gray-scale bar indicates positive and negative values in the difference image.

C. 3rd-order Registration

To further account for differences in cross-sectional orientation and structural deformation in postmortem images (e.g., shrinkage artifacts and ventricle collapse), we increased the order of polynomials up to the 3rd-order. This increases the number of polynomial coefficients (i.e., 18 coefficients in the 2nd-order model vs. 30 in the 3rd-order) and adds complications to the estimation procedure. The third order transformation is expected to improve the coregistration for those cases with more severe distortions in postmortem slices.

Fig. 7 shows a representative result using the 3rd-order polynomial transformation. Compared to the 2nd-order transformation, improved registration is noticed in several gyri, and collapsed ventricles are better matched in the registered image. These effects are also visible in the difference images shown in Figs 7(d) and (e) corresponding to the 2nd and 3rd-order transformations respectively. The value of MSE at convergence using the 2nd-order registration was 1.28E5 and dropped to 3.3E4 using the 3rd-order. In terms of spatial correlation coefficient between the postmortem and registered MRIs, the cc value increased from 0.899 (2nd-order) to 0.906 (3rd-order). These numbers suggest significantly improved registration with 3rd-order transformation. The statistical significance level for this difference in correlation coefficients between the second and third order registrations was 0.0006 using Fisher's Z transformation [14].

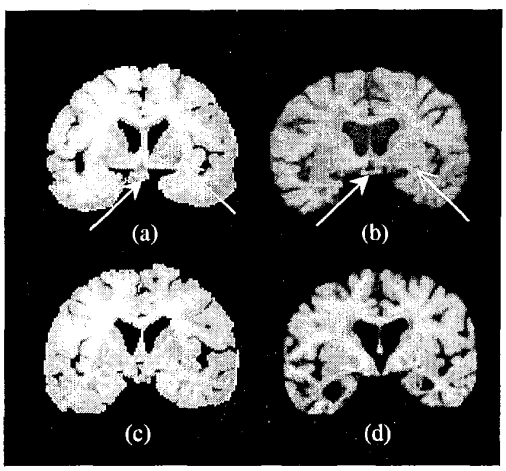

Figure 6: Results of coronal image registration of another subject using 2nd-order registration. (a)-(c) Two consecutive postmortem slices, (b)-(d) registered MRIs to (a) and (c) respectively. Two identical anatomical landmarks are identified: one set of arrows point to the optic chiasm and the other set to the perivasular space in both postmortem and registered MR images.

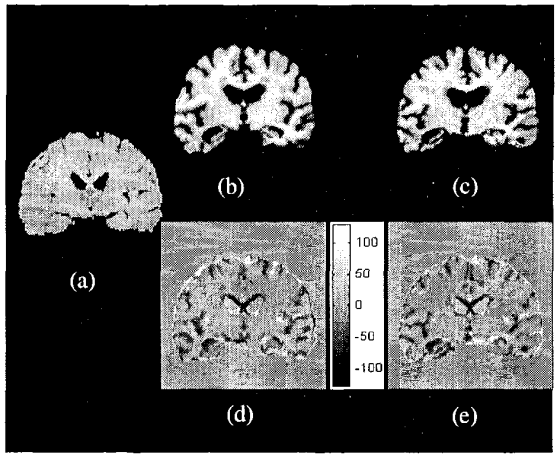

Figure 7: Comparison of 2nd-order and 3rd-order registration. (a) Postmortem slice, (b) registered MR slice using the 2nd-order transformation, and (c) using the 3rd-order transformation. (d) Difference image (b) minus (a). (e) Difference image (c) minus (a).

D. Registration Involving Different Orientations

As an example of registration involving different orientations of slices, we present the results of translating lesions (in this case lacunes) found in a transaxial MRI slice to a coronal postmortem slice. We identified a region of lacunar infarct shown as a small white patch in Fig. 8 (a) on a T2-weighed transaxial MR slice. Then this MR slice was registered to the reference T1 weighted MR volume after intensity inversion and voxel size matching (to match the intensity distribution of the reference volume). The registered MR slice is shown in Fig. 8 (b). Based on the registered transformation coefficients, the identified lacune, whose size was approximately 3.4x4.3x6mm^3, was registered into the 3D MR volume. Several postmortem slices were registered to their corresponding 2D warped sections within the MRI volume, till a postmortem slice whose registered MR section contained the marked lesion in 3D volume was found. The warped MRI section containing the lacune is shown in Fig. 8 (c) and the corresponding postmortem slice is shown in Fig. 8 (d). An analysis of the coordinates indicates that the centroid of the region identified as a lacune in the postmortem slice matches the centroid of the lacune identified in the MRI section to an accuracy of 1 ± 0.5 pixels. The position of the lacune in the postmortem slice is indicated by an arrow in Fig. 8 (e).

The results of this study demonstrate the flexibility of the slice-to-slice registration approach while maintaining the high sensitivity of registration. The reverse of these procedures is also possible. For instance, the ROI in postmortem images that cannot be readily identified in MRI can be spatially translated and registered to its corresponding locations in any orientation of MRI slices.

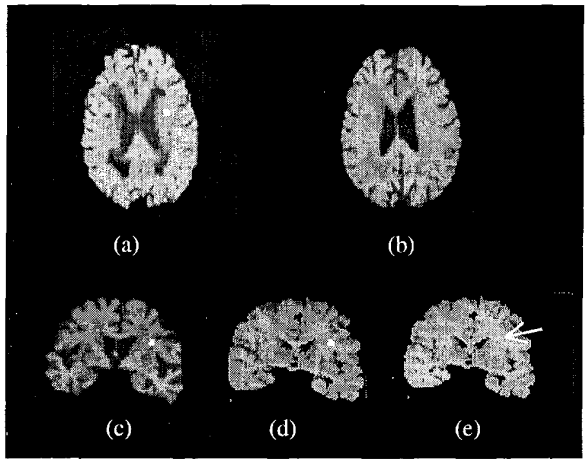

Figure 8: Registration in different orientation. (a) Lesion is marked in white on a T2-weighted transaxial MR slice. (b) Registered T1-weighted transaxial slice derived from the 3D reference volume to match (a) using the 2nd-order polynomial transformation, (c) warped MR section registered to a coronal postmortem slice shown in (d). The lesion found in (a) and translated into (c) is mapped into (d). (e) Original postmortem slice where an arrow indicates an identified lacune.

IV. Discussion

The inspection of postmortem images can provide information at the cellular level about a disease through cell counting. To quantify pathology more objectively, monitoring the natural progression of a disease over a period of time is critical. Since routinely acquired MR images provide such measures, accurate registration of postmortem slices to their corresponding MR slices would be useful.

Most registration schemes currently available address problems in either the same imaging modality such as MRI-to-MRI or cross imaging modalities such as MRI-to-PET [8].

Although a technique developed by Thompson and Toga [7] addresses the registration problem of postmortem images to MRI, their techniques require very sophisticated setups for postmortem brain preparation through, not readily available, cryo-sectioning [7] and high-level of digitization to reconstruct a high resolution 3D postmortem brain volume. Furthermore their warping mechanism is computationally demanding and time-consuming, although high-degree of local correlation might be possible through their physical continuum models [7].

The significance of our approach lies in its practicability, high sensitivity, cost-effectiveness, and automatic features to minimize expert human intervention such as landmark localization, slice realignment, or structural model generation. The practicability is preserved since the technique does not require sophisticated preparation of postmortem slices and compensates geometrical distortions nonlinearly via global deformation of n^{th}-order polynomials. Since the slice-to-slice matching scheme does not require a high-resolution postmortem volume and in general ROIs only reside in a few postmortem slices, only the desired slices can be registered by maximizing the correlation of a particular slice, thus maintaining maximum sensitivity of that slice.

Regarding the order of non-linear transformation, we have tested the polynomial transformation up to the 3^{rd}-order. However it is not clear that further expansion of polynomial order would perform better coregistration. Since higher order of polynomials complicates parameter estimation and demands more computation time, the trade-off between model order and registration performance must be investigated. In the case of MRI-to-MRI registration where structural deformation is not significant, Woods et al. [8] showed marginal improvement of registration with higher number of coefficients. The performance of high model order generally depends on the degree of non-linear deformation in postmortem images.

Although mean-squared error is a reliable cost function, it is certainly possible to come up with better registration cost criteria. Recently mutual information was used to measure the statistical dependency of intensity patterns of two different images and it was suggested that the mutual information matrix is more suitable for inter-modality image registration [14]. Thus maximizing mutual information may become a better objective function. We are currently investigating its feasibility.

The merit of non-linear polynomial transformations is the ability to do spatial transformation with a specified order. Although this should provide enough freedom to produce non-linear warping, a local refining registration mechanism might be needed to improve the registration accuracy of local regions. One way to maximize the freedom of local deformations is by adopting a physical continuum model of Thompson and Toga [7] with higher computational burden. At present, to improve local registration at reasonable cost, we are investigating the possibility of utilizing a local window surrounding a specific anatomical region to enable maximization of cross-correlation [10] or mutual information [15] between small windows as a refining procedure after our global slice-to-slice registration.

Although we have attempted to validate our procedure via voxel similarity measures such as MSE and correlation, and anatomical landmarks, we recognize that these measures do not provide direct comparison of brain structures in size and shape. However, one should note that this type of direct validation is difficult in registering postmortem to MRI slices since segmenting and reconstructing common structures of the postmortem brain is not readily possible. Furthermore, as noted by Woods in [7], structure comparison is problematic when nonlinear warping is involved since nonlinear transformation of structure causes distortions that might not exist in nature. This adds complications on top of pathological and geometrical distortions. Currently, we are investigating a method of reconstructing the postmortem brain in 3D, so that we can extract and reconstruct anatomical structures. This might allow us to come up with novel validation criteria such as distances between specific structures to assess registration accuracy.

V. Conclusion

We have presented a new registration method relying on polynomial transformations to correlate postmortem slices to their corresponding MR sections within a MR volume. With this approach, MR characteristics of a disease can be correlated to the pathology of the disease. Our approach in this study is efficient and cost-effective, and can be applied automatically with minimum human intervention.

VI. Acknowledgment

This work is supported in part by grants NIA-NIH 1PO1AG 12453 and NIA-NIH P50 AG05142.

VII. References

[1] H.M. Wisniewski and J. Wegiel, Neuropathology of Alzheimer's disease, *Neuroimaging Clin. N. Am.*, vol. 5, pp.45-57, 1995.

[2] S. Grafton, M. Sumi, G.K. Stimac, E.C. Alvord, C.-M. Shaw, and D. Nochlin, Comparison of postmortem magnetic resonance imaging and neuropathologic findings in the cerebral white matter, *Arch. Neurol.*, vol. 48, pp.293-298, 1991.

[3] Gyorffy-Wagner, E. Englund, E.-M. Larsson, A. Brun, S. Cronqvist, and B. Persson, Proton magnetic resonance relaxation times T1 and T2 related to postmortem interval: An investigation on porcine brain tissue, *Acta Radiol. Diagnosis*, vol. 27, pp.115, 1986.

[4] M. R., Grafe, G. A. Press, D. P. Berthoty, J.R. Hesselink, and C.A. Wiley, Abnormalities of the brain in AIDS patients: Correlation of postmortem MRI findings with neuropathology, *AJNR.*, vol. 11, pp.905-911, 1990.

[5] P.L. McGeer, H. Kamo, R. Harrop, E.G. McGeer, W.R.W. Martin, B.D. Pate, and D.K.B. Li, Comparison of PET, MRI, and CT with pathology in a proven case of Alzheimer's disease, *Neurology*, vol. 36, pp.1569-1574, 1986.

[6] J. R. Nixon, G.M. Miller, H. Okazaki, and M.R. Gomez, Cerebral tuberous sclerosis: Postmortem magnetic resonance imaging and pathologic anatomy, *Mayo Clin. Proc.*, vol. 64, pp.305-311, 1989.

[7] A. W. Toga, Editor, Brain Warping, San Diego: Academic Press, 1999.

[8] R. P. Woods, S. T. Grafton, C. J. Holmes, S. R. Cheery, and J. C. Mazziotta, Automated Image Registration: I. General Methods and Intrasubject, Intramodality Validation, *J. of Computer Assisted Tomography*, vol. 22(1), pp.139-152, 1998.

[9] S. Sandor and R. Leahy, Surface-Based Labeling of Cortical Anatomy Using a Deformable Atlas, *IEEE Trans. Med. Img.*, vol. 16(1), pp.41-54, 1997.

[10] M. Singh, W. Frei, and T. Shibata, A digital technique for accurate change detection in nuclear medicine images with applications to myocardial perfusion studies using thallium-201, *IEEE Trans. Nucl. Sci.,* vol. 26, pp.565-575, 1979.

[11] W. H. Press, S. A. Teukolsky, W. T. Vetterling, and B. P. Flannery, Numerical Recipes, Cambridge: University Press, 1992.

[12] M. Singh, L. Al-Dayeh, P. Patel, and T. Kim, Correction of Head Movements in Multi-Slice EPI and Single-Slice Gradient-Echo Functional MRI, *IEEE Trans. Nucl. Sci.*, vol. 45, pp.2162-2167, 1998.

[13] M. Holden, D.L.G. Hill, E.R.E. Denton, J.M. Jarosz, T.C.S. Cox, T. Rohlfing, J. Goodey, and D.J. Hawkes, Voxel Similarity Measures for 3-D Serial MR Brain Image Registration, *IEEE Trans. Med. Img.,* vol. 19, pp.94-102, 2000.

[14] N.M. Downie and R.W. Heath, Basic Statistical Methods, Harper & Row Publishers, New York, 1970.

[15] B. Kim, J. L. Boes, K. A. Frey, and C. R. Meyer, Mutual information for automated unwarping of rat brain autoradiography, *Neuroimage*, vol. 5(1), pp.31-40, 1997.